Inorganic Chemistry

Article

pubs.acs.org/IC

NH_3-Promoted Ligand Lability in Eleven-Vertex Rhodathiaboranes

Beatriz Calvo,[†] Beatriz Roy,[†] Ramón Macías,*[,†] Maria Jose Artigas,[†] Fernando J. Lahoz,[†] and Luis A. Oro[†,‡]

[†]Departamento de Química Inorgánica, Instituto de Síntesis Química y Catálisis Homogénea, Universidad de Zaragoza-CSIC, 50009-Zaragoza, Spain

[‡]King Fahd University of Petroleum and Minerals, KFUPM Visiting Professor, Dhahran 31261, Saudi Arabia

Supporting Information

ABSTRACT: The reaction of the 11-vertex rhodathiaborane, [8,8-$(PPh_3)_2$-*nido*-8,7-$RhSB_9H_{10}$] (**1**), with NH_3 affords inmediately the adduct, [8,8,8-$(NH_3)(PPh_3)_2$-*nido*-8,7-$RhSB_9H_{10}$] (**4**). The NH_3−Rh interaction induces the labilization of the PPh_3 ligands leading to the dissociation product, [8,8-$(NH_3)(PPh_3)$-*nido*-8,7-$RhSB_9H_{10}$] (**5**), which can then react with another molecule of NH_3 to give [8,8,8-$(NH_3)_2(PPh_3)$-*nido*-8,7-$RhSB_9H_{10}$] (**6**). These clusters have been characterized in situ by multielement NMR spectroscopy at different temeperatures. The variable temperature behavior of the system demonstrates that the intermediates **4**−**6** are in equilibrium, involving ligand exchange processes. On the basis of low intensity signals present in the ^1H NMR spectra of the reaction mixture, some species are tentatively proposed to be the *bis*- and *tris*-NH_3 ligated clusters, [8,8-$(NH_3)_2$-*nido*-8,7-$RhSB_9H_{10}$] (**7**) and [8,8,8-$(NH_3)_3$-*nido*-8,7-$RhSB_9H_{10}$] (**8**). After evaporation of the solvent and the excess of NH_3, the system containing species **4**−**8** regenerates the starting reactant, **1**, thus closing a stoichiometric cycle of ammonia addition and loss. After 40 h at room temperature, the reaction of **1** with NH_3 gives the hydridorhodathiaborane, [8,8,8-$(H)(PPh_3)_2$-*nido*-8,7-$RhSB_9H_9$] (**2**), as a single product. The reported rhodathiaboranes show reversible H_3N-promoted ligand lability, which implies weak Rh−N interactions, leading to a rare case of metal complexes that circumvent "classical" Werner chemistry.

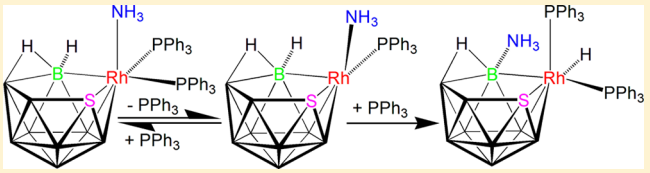

INTRODUCTION

The homogeneous catalysis of reactions between organic molecules and ammonia is very attractive because it provides a direct access to nitrogen-containing products. However, there are few examples of homogeneous catalytic functionalization of NH_3.[1] One of the main reasons behind the difficulties of NH_3 activation is the fact that ammonia forms inert Werner-type Lewis acid−base adducts.[2] Thus, the investigation of systems featuring weak-bonding interactions with NH_3 is of interest because this could enhance the reactivity of ammonia,[3] leading to its activation, through, for example, formation of amido complexes ($M-NH_2$), which are believed to be intermediates in catalytic reactions with ammonia.[4]

Polyhedral boron-containing compounds are well suited to the search for new forms of interactions with ammonia and its potential functionalization. Since ammonia is an effective Lewis base, it forms NH_3−borane adducts.[5] Small ammonia−borane adducts such as H_3NBH_3 and $H_3NB_3H_7$ have attracted increasing attention as chemical hydrogen storage materials.[6] This has sparked a considerable interest in the catalytic dehydrogenation and oxidative-hydrolysis of these materials, affording new mechanistic insights.[7] These studies represent examples of borane/metal fragment cooperation leading to the transformation of ammonia. The combination of transition metal complexes and boranes gives rise to the question as to how the H_3N-B and metal moieties would behave if it were possible for them to act in concert as an integral part of a single reagent and also what would be the potential NH_3−metal interactions.

Metallaboranes and metallaheteroboranes containing M−B, B−B, and B−H bonds provide vehicles for answering these questions experimentally. We report here 11-vertex rhodathiaboranes capable of circumventing "classical" Werner chemistry, leading to a rare case of a reversible H_3N-promoted ligand lability, which implies a weak Rh−N bonding interaction. This reactivity augurs well for the potential catalytic functionalization of ammonia, and it provides good grounds for future studies on NH_3−borane/metal cooperation.

RESULTS AND DISCUSSION

Reactions of [8,8-$(PPh_3)_2$-*nido*-8,7-$RhSB_9H_{10}$] (1) with NH_3. The treatment of the 11-vertex rhodathiaborane [8,8-$(PPh_3)_2$-*nido*-8,7-$RhSB_9H_{10}$] (**1**)[8] with excess ammonia affords, after 48 h, the NH_3-ligated hydridorhodathiaborane, [8,8,8-$(H)(PPh_3)_2$-9-(NH_3)-*nido*-8,7-$RhSB_9H_9$] (**2**). This polyhedral compound results from ammonia binding to the cluster B(9) vertex and conconmitant migration of a hydrogen atom to the rhodium center. In this, therefore, it resembles the reaction of **1** with pyridine.[9] As illustrated in Scheme 1, the hydride ligands in these reactions quite likely arise from the migration of the

Received: July 25, 2014
Published: November 10, 2014

   dx.doi.org/10.1021/ic501779n | *Inorg. Chem.* 2014, 53, 12428−12436

Scheme 1. Reaction of Compound 1 with Ammonia

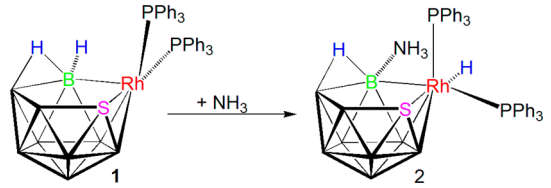

hydrogen atom either at the B(9)−H vertex or along the B(9)−B(10) edge to the rhodium center in **1**.

Compound **2** has been characterized by multielement NMR spectroscopy and by X-ray diffraction analysis. Figure 1 depicts

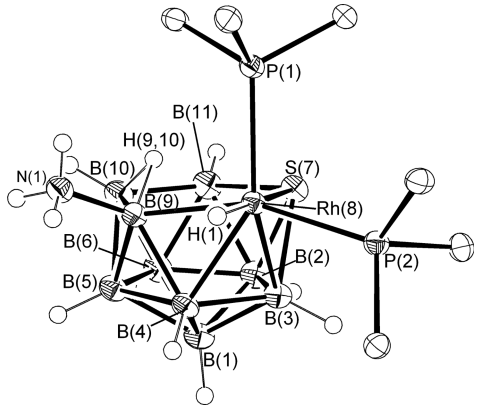

Figure 1. Molecular structure of [8,8,8-(H)$(PPh_3)_2$-9-(NH_3)-*nido*-8,7-$RhSB_9H_9$] (**2**).

an ORTEP-type drawing of this molecule, and Table 1 lists some selected angles and distances for **2** together with its pyridine-ligated counterpart, [8,8,8-(H)$(PPh_3)_2$-9-(NC_5H_5)-*nido*-8,7-$RhSB_9H_9$] (**3**).

The molecular structure of **2** is based on an 11-vertex cluster that can formally be derived from an icosahedron by the removal of a vertex, leading to the formation of a pentagonal face. The main structural features of this metallathiaborane are the presence of a bridging hydrogen atom along the B(9)−B(10) edge, an NH_3 substituent bound to the B(9) vertex, and an $\{Rh(H)(PPh_3)_2\}$ group at the 8-vertex of connectivity four. The Rh−H hydride ligand was located by using the program HYDEX,[10] and its coordinates were subsequently refined against the X-ray data. The compound is classified as nido, conforming to the structure predicted for an 11-vertex cluster with 13 skeletal electron pairs.[11]

The *exo*-polyhedral configuration at the rhodium center is directed by the sulfur atom, which drives the hydride ligand trans to the S(7) position. This ligand orientation leads to the most stable $\{Rh(H)(PPh_3)_2\}$-to-$\{\eta^4$-$SB_9H_9(NH_3)\}$ configuration because the strong trans-effect hydride ligand lies trans to the weakest trans-effect vertex of the $\{\eta^4$-S(7)B(3)B(4)B(9)$\}$ face.[12]

Overall, the distances and angles found in compound **2** are similar to those for the pyridine analogue, **3** (Table 1). It is, however, noteworthy that the Rh(8)−P(2) distance at 2.3891(6) Å is significantly longer than that found in **3** [2.354(2)] suggesting a stronger structural *trans*-effect of the B(9)-NH_3 vertex than the B(9)-NC_5H_5 unit. The B(9)−N(1) length at 1.571 Å is close to the average value 1.536 Å found for this bond (CSD rearch using the B−N single bond as query:

Table 1. Selected Interatomic Distances (Å) and Angles (deg) with Estimated Standard Uncertainties (s.u.) in parentheses for [8,8,8-(H)$(PPh_3)_2$-9-(NH_3)-*nido*-8,7-$RhSB_9H_9$] 2 and [8,8,8-(H)$(PPh_3)_2$-9-(NC_5H_5)-*nido*-8,7-$RhSB_9H_9$] 3[9a]

	2[a]	3[a]
Rh(8)−S(7)	2.4295(6) [2.5556]	2.431(2) [2.535]
Rh(8)−P(1)	2.3370(6) [2.4448]	2.341(2) [2.526]
Rh(8)−P(2)	2.3891(6) [2.5123]	2.354(2) [2.387]
Rh(8)−B(3)	2.259(3) [2.307]	2.201(10) [2.311]
Rh(8)−B(4)	2.226(3) [2.249]	2.217(11) [2.253]
Rh(8)−B(9)	2.198(3) [2.185]	2.220(9) [2.223]
S(7)−B(2)	1.992(3) [2.003]	1.980(9) [1.998]
S(7)−B(3)	2.040(3) [2.061]	2.059(11) [2.059]
S(7)−B(11)	1.935(3) [1.948]	1.953(9) [1.939]
N(1)−B(9)	1.571(4) [1.600]	1.547(11) [1.569]
B(2)−B(3) (longest)	1.904(4) [1.905]	1.906(14) [1.905]
B(6)−B(11) (shortest)	1.745(4) [1.737]	1.727(14) [1.737]
B(9)−B(10)	1.866(4) [1.850]	1.7845(14) [1.865]
P(1)−Rh(8)−P(2)	102.14(2) [101.27]	100.27(7) [100.54]
S(7)−Rh(8)−P(1)	94.10(2) [96.69]	96.38(7) [97.26]
S(7)−Rh(8)−P(2)	101.06(2) [103.74]	102.05(8) [105.27]
Rh(8)−B(9)−N(1)	121.04(17) [117.84]	120.6(5) [118.8]
P(1)−Rh(8)−B(9)	97.93(7) [97.28]	95.8(3) [154.7]
P(2)−Rh(8)−B(9)	157.37(7) [160.25]	162.4(3) [100.1]
S(7)−Rh(8)−B(9)	87.72(7) [85.32]	87.1(3) [86.4]

[a]Values for the DFT-optimized structures are given between brackets.

found in 10 658 hits).[13] There are 13 boron-based polyhedral structures reported in the Cambridge Structural Database (CSD) that feature a NH_3 substituent bound to a boron vertex; and between them, none incorporates a metal center in the cage: they are boranes. The hydridorhodathiaborane here is, as far as we are aware, the first crystallographically characterized metallaborane featuring a B−NH_3 group.

The ^{11}B NMR spectrum of **2** exhibits seven signals of relative intensity ratio 1:1:2:1:2:1:1 between δ_B +10.2 and −30.2 ppm. The DFT GIAO-calculated values span the same interval, matching the experimental data, and, therefore, providing a good theoretical model for the hydridorhodathiaborane. It is interesting to note that the resonance for the NH_3-substituted boron atom shifts ca. 10 ppm to lower frequency when compared to the pyridine-ligated analogue, **3**. A shift to lower frequency is also found for the ^{1}H resonance of the B−H−B bridging hydrogen atom in **2** (δ_H −2.50 ppm) compared to **3** (δ_H −1.53 ppm). These differences in the proton resonance could be ascribed to the deshielding effects of the pyridine π-electron current in **3**, which are absent in **2**; however, other electronic effects such as, for example, the fact that ammonia is a better σ-donor than the pyridine ligand, should be invoked to explain the large deshielding observed on the boron nucleus of the pyridine-ligated cluster, **3**.

As indicated above, **2** is formed several hours after the addition of NH_3 to a solution of **1**. This is illustrated in Figure 2. The spectrum in the bottom trace (Figure 2a) exhibits a broad doublet at δ_P +38.0 that corresponds to different species in solution that undergo fast ligand exchange (vide infra). This system evolves further to afford **2**. Thus, after 24 h (Figure 2b), the ^{31}P-{^{1}H} NMR spectrum at 298 K exhibits a doublet of doublets at δ_P +39.7 and a very broad peak at +28.0 that correspond to the hydridorhodathiaborane, **2**, which now is the major product in solution.

dx.doi.org/10.1021/ic501779n | *Inorg. Chem.* 2014, 53, 12428−12436

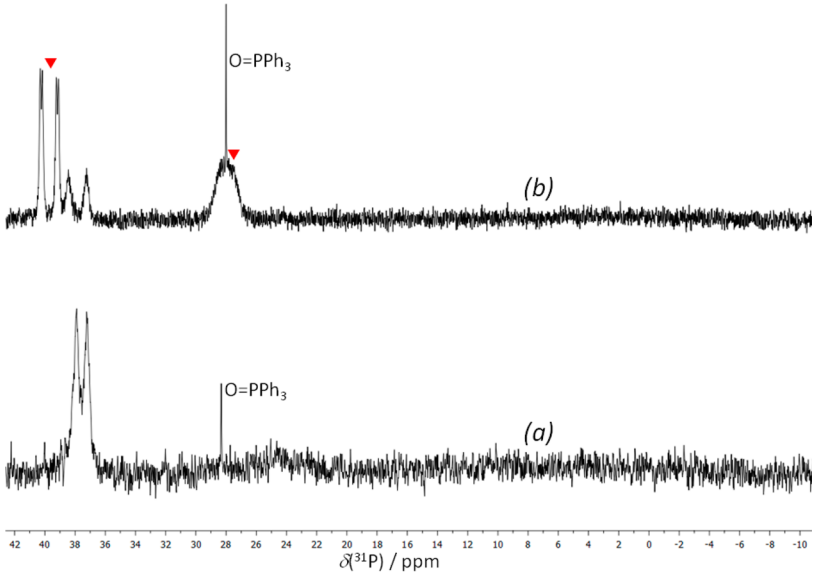

Figure 2. $^{31}P\text{-}\{^{1}H\}$ spectra in CD_2Cl_2 at room temperature: (a) few hours after the addition of NH_3 to **1** in CD_2Cl_2; (b) after 24 h in solution in the presence of excess of ammonia. The signals corresponding to **2** are marked with red triangles. The broad doublet at δ_P +38.0 corresponds to different species undergoing fast ligand exchange.

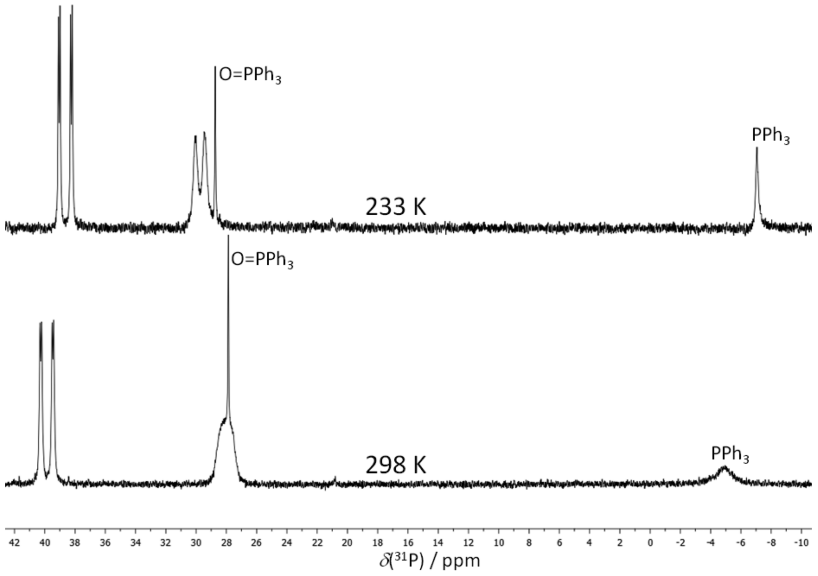

Figure 3. $^{31}P\text{-}\{^{1}H\}$ spectra in CD_2Cl_2 of **2** and free PPh_3 at 298 and 233 K.

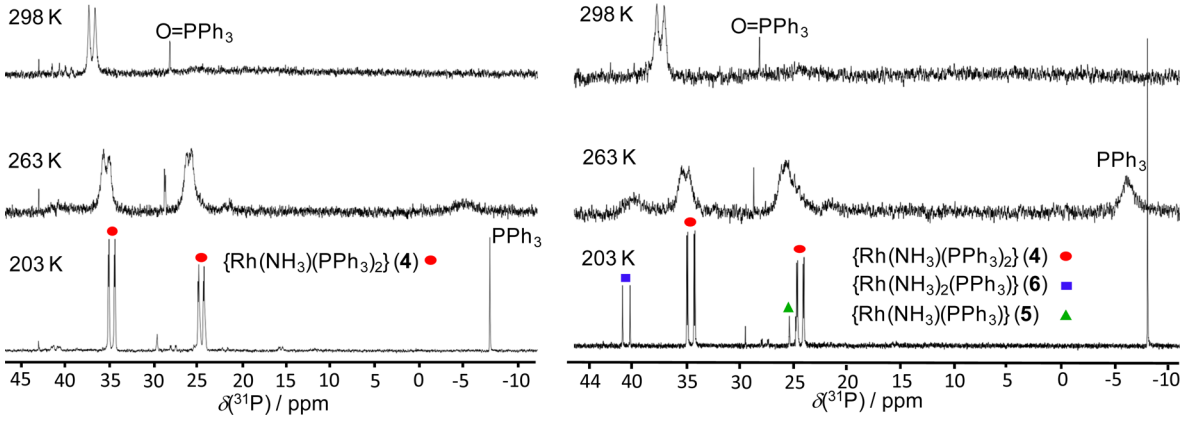

Figure 4. $^{31}P\text{-}\{^{1}H\}$ VT NMR spectra, after the exposure of **1** to 2 bar of NH_3 for 10 s at 243 (left) and at 203 K (right).

dx.doi.org/10.1021/ic501779n | *Inorg. Chem.* 2014, 53, 12428−12436

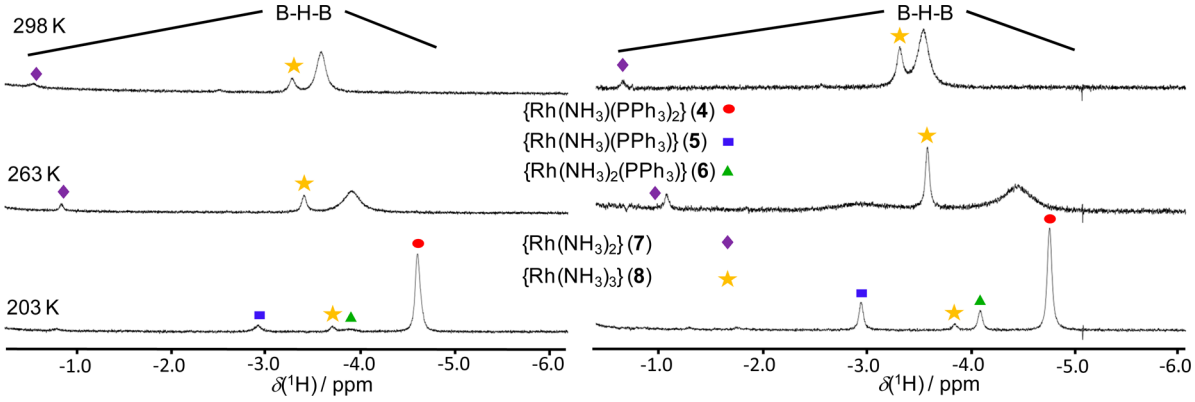

Figure 5. VT ^{1}H-{^{11}B} NMR spectra and at low temperatures, following the exposure of **1** to 2 bar of NH_3 for 10 s at 243 (left) and at 203 K (right).

Figure 3 shows the ^{31}P-{^{1}H} NMR spectra of **2** in the presence of free PPh_3 at different temperatures. As the temperature is lowered, the resonance at δ_P +28.0 ppm becomes a broad doublet, whereas the signal of the free PPh_3 sharpens significantly. This variable temperature (VT) NMR behavior suggests that one of the PPh_3 ligands in **2** is undergoing ligand exchange. Similar VT broadening in the ^{31}P-{^{1}H} NMR spectrum was observed for the pyridine-ligated counterpart, **3**;[9] although, ligand exchange with free PPh_3 was not apparent in this system, thus indicating a lower dissociative lability than the NH_3-ligated cluster **2**.

VT NMR Studies. The study at low temperatures of the reaction between a CD_2Cl_2 solution of **1** and NH_3 has allowed the characterization of different intermediates in solution. Thus, the exposure of **1** to 2 bar of NH_3 in a quick pressure valve NMR tube at 243 K yields an instant color change from red to bright yellow. The ^{31}P-{^{1}H} NMR spectrum of this sample at 203 K shows two doublets of doublets and free phosphine in a 1:1:0.2 relative intensity ratio. The signals broaden and coalesce at room temperature into a doublet δ_P at +37.3 (Figure 4).

Interestingly, if the NMR tube containing a CD_2Cl_2 solution of **1** is cooled to 203 K and then exposed to 2 bar of NH_3, the results are quite different. The ^{31}P-{^{1}H} NMR spectrum now exhibits two new doublets at +40.7 and +25.2 ppm together with the previously observed doublets of doublets and free PPh_3. As the temperature is increased, all the ^{31}P resonances broaden and coalesce at room temperature to give a doublet at +37.2 ppm (Figure 4).

It is important to note that the exposure of **1** to the 2 bar atmosphere of ammonia at 203 and 243 K for the same time, affords different ammounts of NH_3 in solution. Thus, at 203 K the condensation of ammonia in the quick pressure valve NMR tube is higher than at 243 K, resulting in higher concentrations of NH_3. This can be seen in the corresponding ^{1}H NMR spectra.

If we compare the corresponding ^{1}H–{^{11}B} NMR data of both samples (Figure 5), we observe that the system prepared at 243 K yields a spectrum exhibiting a high intensity peak at δ_H −4.60 ppm together with low intensity resonances at δ_H −0.78, −2.92, −3.70, and −3.89 ppm. As the temperature is increased, the resonances broaden, yielding, at room temperature, broad resonances at δ_H −3.41 and −3.71 ppm in a 1:4 relative intensity ratio. The sample prepared at 203 K also shows four peaks at δ_H −2.92, −3.83, −4.08, and −4.74 ppm in a 0.14:0.01:0.13:1 relative intensity ratio. These resonances resemble the spectrum of the 243 K sample, but with different relative intensities. As the temperature is increased, the signals in the proton spectrum broaden and coalesce to give the same pattern in the negative region as that of the sample prepared at 243 K.

These NMR data demonstrate that the reactivity of **1** with NH_3 depends both on the concentration of ammonia and on the temperature, giving different species that are in equilibrium. The ^{1}H NMR signals can be assigned to the B–H–B bridging hydrogen atom along the B(9)–B(10) edge on the pentagonal face of different 11-vertex *nido*-rhodathiaboranes.

Table 2 gathers the ^{1}H chemical shifts assigned to the B–H–B bridging hydrogen atoms of some {RhL_3} *tris*-ligated and {RhL_2} *bis*-ligated 11-vertex *nido*-rhodathiaboranes. These data demonstrate that the addition of a third ligand to the formally unsaturated rhodium center in the parent *bis*-$(L)_2$-ligated rhodathiaboranes, leads to a large low-frequency shift in the B–H–B bridging proton resonance.[14] Thus, this large shift is diagnostic of the formation of {RhL_3} *tris*-ligated 11-vertex species versus their {RhL_2} *bis*-ligated counterparts. Based on

Table 2. ^{1}H Chemical Shifts of the B–H–B Bridging Hydrogen Atom in Some {RhL_2} *bis*- and {RhL_3} *tris*-Ligated Rhodathiaboranes

compound[a]	δ_H/ppm	ref
{RhL_2} bis-ligated		
[8,8-$(PPh_3)_2$-*nido*-8,7-$RhSB_9H_{10}$] (**1**)	−1.32	8
[8,8-$(PMe_2Ph)_2$-*nido*-8,7-$RhSB_9H_{10}$]	−1.30	14
[8,8-$(PMe_3)_2$-*nido*-8,7-$RhSB_9H_{10}$]	−1.33	14
[8,8-$(py)_2$-*nido*-8,7-$RhSB_9H_{10}$]	−0.70	15
[8,8-(phen)-*nido*-8,7-$RhSB_9H_{10}$]	−0.36	15
[8,8-(Me_2bpy)-*nido*-8,7-$RhSB_9H_{10}$]	−0.64	15
[8,8-(bpy)-*nido*-8,7-$RhSB_9H_{10}$]	−0.78	15
[8,8-$(NH_3)(PPh_3)$-*nido*-8,7-$RhSB_9H_{10}$] (**5**)	−2.92	this work
[8,8-$(NH_3)_2$-*nido*-8,7-$RhSB_9H_{10}$] (**7**)	−0.78	this work
{RhL_3} tris-ligated		
[8,8,8-$(PMe_2Ph)_3$-*nido*-8,7-$RhSB_9H_{10}$]	−3.98	14
[8,8,8-$(PMe_3)_3$-*nido*-8,7-$RhSB_9H_{10}$]	−3.75	14
[8,8,8-$(CO)(PPh_3)_2$-*nido*-8,7-$RhSB_9H_{10}$]	−3.85	16
[8,8,8-(phen)(PPh_3)-*nido*-8,7-$RhSB_9H_{10}$]	−2.02	15
[8,8,8-(Me_2bpy)(PPh_3)-*nido*-8,7-$RhSB_9H_{10}$]	−2.22	15
[8,8,8-(bpy)(PPh_3)-*nido*-8,7-$RhSB_9H_{10}$]	−2.13	15
[8,8,8-$(NH_3)(PPh_3)_2$-*nido*-8,7-$RhSB_9H_{10}$] (**4**)	−4.60	this work
[8,8,8-$(NH_3)_2(PPh_3)$-*nido*-8,7-$RhSB_9H_{10}$] (**6**)	−4.08	this work
[8,8,8-$(NH_3)_3$-*nido*-8,7-$RhSB_9H_{10}$] (**8**)	−3.83	this work

[a]py = pyridine, bpy = 2,2′-bipyridine, Me_2bpy = 4,4′-dimethyl-2,2′-bipyridine, phen = phenanthroline

dx.doi.org/10.1021/ic501779n | *Inorg. Chem.* 2014, 53, 12428−12436

Scheme 2. (a) Proposed Equilibria Studied in CD_2Cl_2 Solution at Room and Low Temperatures; (b) Evaporation under Vacuum[a]

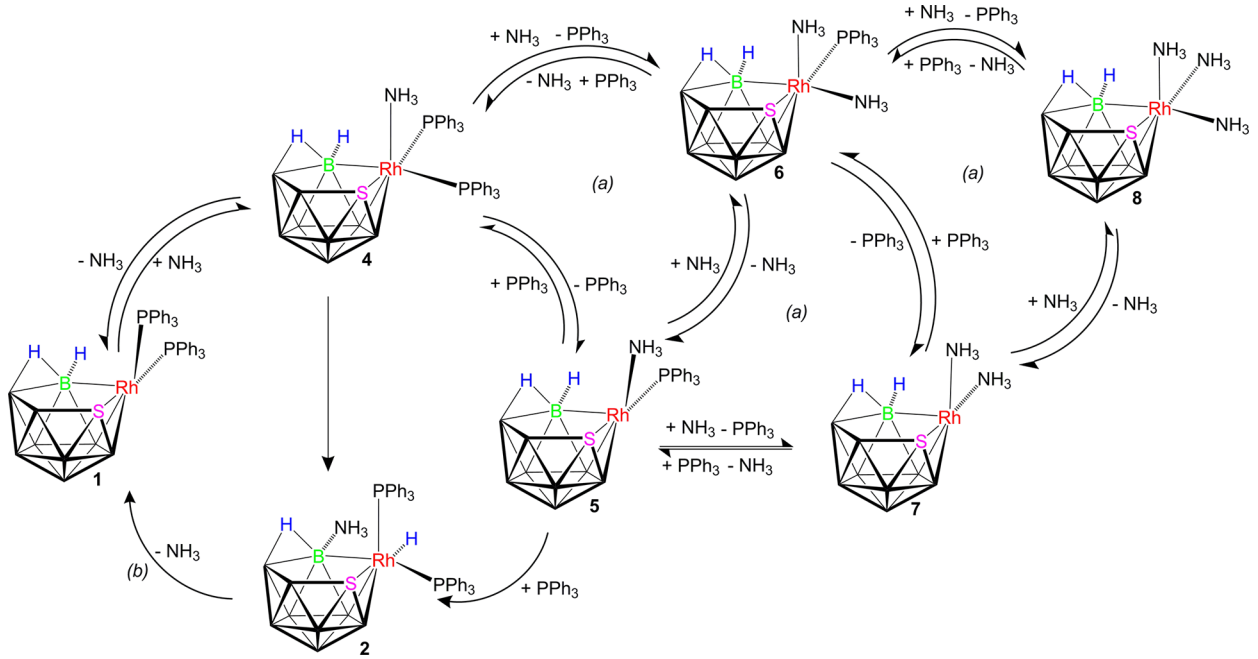

[a]The table lists the ^1H chemical shifts assigned to the B−H−B bridging hydrogen atoms on the pentagonal face of the proposed nido-species.

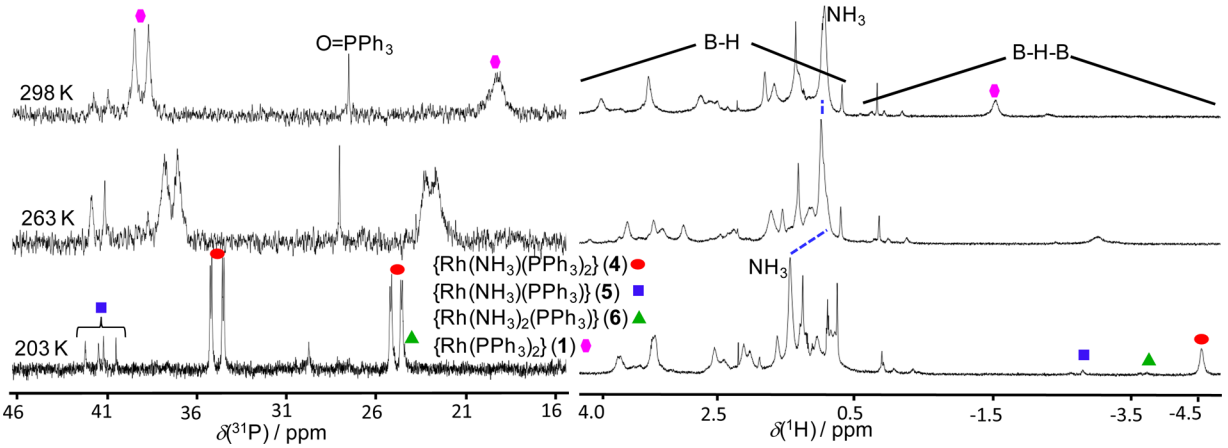

Figure 6. VT $^{31}P-\{^1H\}$ and $^1H-\{^{11}B\}$ spectra of $[8,8,8\text{-}(NH_3)(PPh_3)_2\text{-}8,7\text{-}RhSB_9H_{10}]$ (**4**).

these considerations and the NMR data described above, we propose that NH_3 reacts with **1** to give the metal adduct, $[8,8,8\text{-}(NH_3)(PPh_3)_2\text{-}8,7\text{-}RhSB_9H_{10}]$ (**4**) (Scheme 2 includes a table with the ^1H chemical shift for the bridging hydrogen atom). The two doublets of doublets in the $^{31}P\text{-}\{^1H\}$ spectrum and the proton resonance at the lowest frequency in the $^1H-\{^{11}B\}$ spectrum can be assigned to compound **4**. At low temperature, a PPh_3 ligand is released to give *bis*-$(NH_3)(PPh_3)$-ligated species of formulation, $[8,8\text{-}(NH_3)(PPh_3)\text{-}nido\text{-}8,7\text{-}RhSB_9H_{10}]$ (**5**). Since ammonia is in excess in the reaction medium, a second NH_3 ligand can react with either **4** or **5**, affording *tris*-$(NH_3)_2(PPh_3)$-ligated $[8,8,8\text{-}(NH_3)_2(PPh_3)\text{-}nido\text{-}8,7\text{-}RhSB_9H_{10}]$ (**6**). The resonance of the B−H−B bridging proton in the $\{RhL_3\}$ *tris*-ligated 11-vertex *nido*-rhodathiaborane is expected to shift toward low frequencies with respect $\{RhL_2\}$ *bis*-ligated derivatives, therefore the peaks at δ_H −2.92 and −4.08 ppm are more likely to correspond to **5** and **6**, respectively. Regarding the ^{31}P NMR data at low temperatures, the doublets at δ_P +40.7 and +25.2 ppm could be assigned to either **5** or **6**.

In solution, the proposed clusters, **4**−**6**, undergo intermolecular ligand exchange processes leading to the formation of equilibria. At low temperature, the equilibria shift to the formation of $\{Rh(NH_3)(PPh_3)\}$ **5** and $\{Rh(NH_3)_2(PPh_3)\}$ **6**, as the result of PPh_3 dissociation, and PPh_3 dissociation and addition of one molecule of NH_3 to the metal center in the adduct **4**, respectively. At room temperature, the PPh_3 ligands undergo fast exchange between the rhodium centers of the rhodathiaboranes, **4**−**6**, being averaged into a single doublet (Figures 2 and 4). This dynamic exchange behavior is also demonstrated in the proton NMR spectra where it is clear that the signals corresponding to the B−H−B resonances of the different species broaden and coalesce.

However, in contrast to the ^{31}P NMR spectrum, at room temperature the high field B−H−B proton NMR signals do not average into a single peak but give two high intensity

dx.doi.org/10.1021/ic501779n | *Inorg. Chem.* 2014, 53, 12428−12436

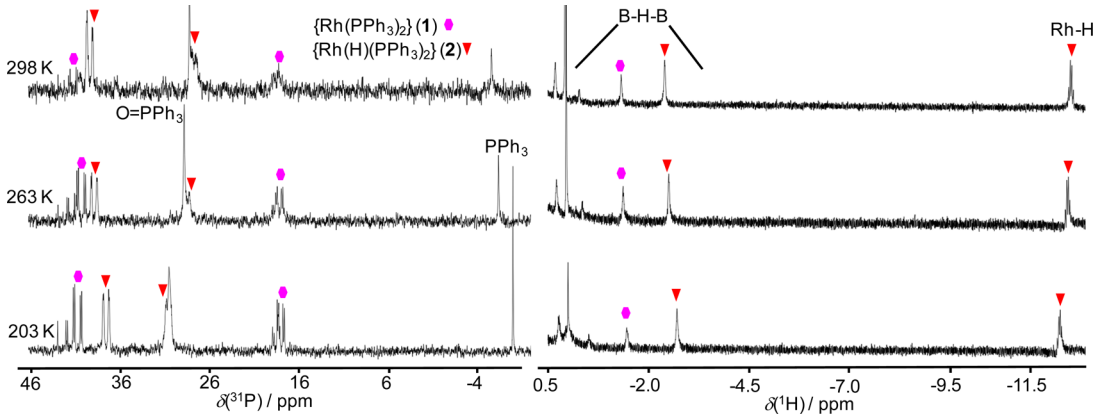

Figure 7. VT ^{31}P-$\{^{1}H\}$ and ^{1}H-$\{^{11}B\}$ spectra of a sample formed after evaporation of a solution formed by [8,8,8-(H)$(PPh_3)_2$-9-(NH_3)-*nido*-8,7-$RhSB_9H_9$] (**2**) and excess of NH_3.

resonances at δ_H −3.2 and −3.6 ppm and a low intensity signal at −0.62 ppm (Figure 5, purple diamond). Species **5**−**6** bear a PPh_3 ligand that, in principle, could react further with excess of NH_3 to give $\{Rh(NH_3)_2\}$ *bis*-ligated and $\{Rh(NH_3)_3\}$ *tris*-ligated species, [8,8-$(NH_3)_2$-*nido*-8,7-$RhSB_9H_{10}$] (**7**) and [8,8-$(NH_3)_3$-*nido*-8,7-$RhSB_9H_{10}$] (**8**). Under this rationale, the B−H−B proton resonances at δ_H −0.62 and −3.29 ppm, in the room temperature spectrum, are tentatively assigned to the *bis*-(NH_3)- and *tris*-(NH_3)-ligated, **7** and **8**, respectively, which at room temperature may undergo slow exchange with PPh_3.

Among all the species proposed to be present in solution, only the *tris*-$(NH_3)(PPh_3)_2$ adduct, **4**, has been isolated as a yellow solid in a 20% yield. The procedure, detailed in the Experimental Section, involves the treatment of a CH_2Cl_2 solution of **1** with NH_3 at low temperature, affording a bright yellow solution that is subsequently overlaid with pentane (or hexane) and kept at 203 K for several days. As the pentane diffuses through the CH_2Cl_2 solution, a yellow precipitate forms. The study of this solid by multielement NMR spectroscopy reproduces the ^{1}H and ^{31}P NMR data found for the previously described 243 K sample measured at 203 K (left spectra in Figures 4 and 5). Thus, the ^{31}P-$\{^{1}H\}$ NMR spectrum exhibits the two doublets of doublets corresponding to compound **4** together with low intensity doublets that may be assigned to the PPh_3-ligated species, **6** and **7**, and some other isomers. It should be noted that the absence of free PPh_3 in this sample indicates that, without excess of NH_3 in solution, the dissociation of one PPh_3 ligand in the *tris*-$NH_3(PPh_3)_2$ adduct **4** is inhibited. At higher temperatures (Figure 6) the two doublets of doublets in the ^{31}P-$\{^{1}H\}$ spectrum broaden significantly and move appart from each other to approach readily the ^{31}P chemical shifts that correspond to the *bis*-PPh_3-ligated parent rhodathiaborane **1**.

Although the ^{31}P-$\{^{1}H\}$ spectrum of **4** at 298 K resembles that of compound **1**, it is important to note that (i) the high frequency resonance is a doublet in the sample of **4** whereas this signal is resolved as a doublet of doublets in a pure sample of **1** and that (ii) the low frequency peak it is much broader for the sample of **4** than for pure compound **1**. This VT NMR behavior is also reproduced in the corresponding ^{1}H−$\{^{11}B\}$ spectra that show the low frequency B−H−B proton resonance at δ_H −4.60 ppm shifting toward higher frequencies to reach the value of δ_H −1.5 ppm, which is close to the B−H−B resonance of δ_H −1.32 ppm in a pure sample of **1**. Lowering the temperature from 298 to 203 K reproduces the NMR spectra of the NH_3-adduct **4**, demonstrating the reversibility of this VT NMR behavior.

These results indicate that at low temperatures the NH_3 ligand binds readily the rhodium center to form the *tris*-$(NH_3)(PPh_3)_2$-ligated rhodathiaborane, **4**, and that at higher temperatures the Rh−NH_3 linkcage is broken to give **1**. In other words, **4** and **1** are in equilibrum through binding and dissociation of ammonia to the metal center:

$$[(PPh_3)_2\text{-nido-}RhSB_9H_{10}](\mathbf{1}) + NH_3 \rightleftharpoons [(NH_3)(PPh_3)_2\text{-nido-}RhSB_9H_{10}](\mathbf{4})$$

The importance of the amount of NH_3 in solution in the ligand exchange processes is clear when we compare the VT NMR data discussed above. Thus, excess of NH_3 promotes the dissociation of PPh_3 from the rhodium center (Scheme 2), leading to fast PPh_3 exchange at room temperature; whereas one equivalent of ammonia, bound to the rhodium center in compound **4** at 203 K, dissociates at 298 K thus leading to an equilibrium.

Interestingly, for samples containing excess of ammonia and the proposed Rh−NH_3 ligated intermediates, **4**−**8**, evaporation to dryness leads to the regeneration of the starting rhodathiaborane **1** (Figures S2 and S3), demonstrating further the reversibility of the interaction between **1** and ammonia. Similarly, the evaporation of samples containing **2** and an excess of ammonia give a residue that exhibits NMR signals corresponding to a mixture of **1**, **2**, and free PPh_3 (Figure 7).

These results demonstrate that the NH_3 ligand is also labile in **2**, and, therefore, capable of undergoing dissociation and regeneration of the parent compound **1** (Scheme 2b).

We have reported that substitution reactions of **1** with PR_3 ligands follow associative mechanisms. The reactivity of this 11-vertex rhodathiaborane with NH_3 confirms that the binding of the entering Lewis base (i.e., PR_3 or NH_3) to the rhodium center precedes the substitution of the PPh_3 ligand. In addition, it is also reasonable to suggest that the formation of **2** and its pyridine-ligated analogue, [8,8,8-(H)$(PPh_3)_2$-9-(NC_5H_5)-*nido*-8,7-$RhSB_9H_9$] (**3**), may follow an associative process that preceeds the migration of the entering ligand to the B(9) vertex, although further mechanistic studies will be required to determine this.

In summary, these observations allow us to describe a stoichiometric cycle that involves equilibria driven by ligand addition/dissociation and release of NH_3 under vacuum

dx.doi.org/10.1021/ic501779n | *Inorg. Chem.* 2014, 53, 12428−12436

(Scheme 2). Transition elements, with few exceptions,[3a] form strong complexes with ammonia, and this is one of the main reasons behind the difficulty found in its activation throughout either stoichiometric or catalytic cycles. Thus, the equilibria and the cycle reported here represent an uncommon case of late transition metal−ligand lability involving PPh_3 and NH_3.

CONCLUSIONS

In the presence of 1 equiv of ammonia, [8,8-$(PPh_3)_2$-8,7-$RhSB_9H_{10}$] (**1**) and [8,8,8-$(NH_3)(PPh_3)_2$-8,7-$RhSB_9H_{10}$] (**4**) are in equilibrium, undergoing NH_3 addition and dissocation. At higer concentrations of ammonia, the adduct **4** dissociates a phosphine to give [8,8-$(NH_3)(PPh_3)$-8,7-$RhSB_9H_{10}$] (**5**); the presence of an excess of NH_3 gives rise to the formation of other NH_3-ligated species such as [8,8-$(NH_3)_2(PPh_3)$-8,7-$RhSB_9H_{10}$] (**6**). These species are in equilibrium undergoing ligand dissocioation/ligand exchange reactions. The ammonia ligand in these Rh−NH_3 ligated clusters and in the B−NH_3 containing hydridorhodathiaborane, **2**, can be removed under vacuum, regenerating the starting reagent, **1**, and closing a rare stoichiometric cycle of NH_3 addition to/release from polyhedral boron-containing compounds.

Reversible reactions and stoichiometric cycles are central to catalysis, and, given the importance of NH_3 activation for its use in catalytic reactions, the herein reported NH_3-promoted reactivity may give new opportunities for the development of processes leading to the combination of ammonia with organic molecules.

EXPERIMENTAL SECTION

General Procedures. Reactions were carried out under an argon atmosphere using standard Schlenk-line techniques. Dry solvents were obtained from a Solvent Purification System of Innovative Technology Inc. The 11-vertex rhodathiaborane **1** was prepared according to the literature methods.[9] NMR spectra were recorded on Bruker Avance 300-MHz and AV 400-MHz spectrometers, using ^{31}P-{^1H}, ^{11}B, ^{11}B-{^1H}, ^1H, ^1H-{^{11}B}, and ^1H-{^{11}B(selective)} techniques. Residual solvent protons were used as reference (δ, ppm, CD_2Cl_2, 5.32). ^{11}B chemical shifts are quoted relative to [$BF_3(OEt)_2$)], and ^{31}P chemical shifts are quoted relative to 85% aqueous H_3PO_4. Mass spectrometric data were recorded on a high resolution MicroToF-Q instrument operating in negative mode, using CH_3CN as solvent and electrospray ionization.

X-ray Crystallography. An orange-red solution of compound **2** in dichloromethane, containing an excess of NH_3, was filtered through a 0.2 μm PTFE membrane filter via cannula under argon to give a bright yellow solution. The slow diffusion of hexane into this CH_2Cl_2 solution gave crystals of **2** sutable for X-ray diffraction analysis. X-ray diffraction data (Table 3) were collected at low temperature [100(2) K] on an automatic Bruker Kappa APEX DUO CCD area detector diffractometer equipped with graphite-monochromatic Mo−Kα radiation (λ = 0.71073 Å) using narrow frames (0.3° in ω). A single crystal was mounted on a fiber which was covered with a protective perfluoropolyether. Intensities were integrated including Lorentz and polarization effect with SAINT-Plus program[17] and corrected for absorption using multiscan methods applied with SADABS program.[18] The structure was solved using the SHELXS-97 program.[19] Refinements were carried out by full-matrix least-squares on F^2 with SHELXL-97,[20] including isotropic and subsequent anisotropic displacement parameters for all non-hydrogen atoms. The hydride ligand was included from electrostatic potential calculations (HYDEX Program)[10] and freely refined. Regarding the boron-ligated hydrogen atoms, they were observed in Fourier difference map, included in the model in the observed positions, and freely refined.

Calculations. Calculations were performed using the Gaussian 03 package.[21] Structures were initially optimized using standard methods with the STO-3G* basis-sets for C, B, P, S, and H with the LANL2DZ basis-set for the rhodium atom. The final optimizations, including frequency analyses to confirm the true minima, together with GIAO nuclear-shielding calculations, were performed using B3LYP methodology, with the 6-31G* and LANL2DZ basis-sets. The GIAO nuclear shielding calculations were performed on the final optimized geometries and computed ^{11}B shielding values were related to chemical shifts by comparison with the computed value for B_2H_6, which was taken to be $\delta(^{11}B)$ +16.6 ppm relative to the $BF_3(OEt_2)$ = 0.0 ppm standard.

[8,8,8-(H)(PPh_3)-9-(NH_3)-nido-8,7-$RhSB_9H_9$] (**2**). A quick pressure valve NMR tube was charged with a CD_2Cl_2 solution of [8,8-$(PPh_3)_2$-*nido*-8,7-$RhSB_9H_{10}$] (**1**) (12.0 mg, 0.016 mmol); and, then, the system was cooled to 243 K in a dry ice/isopropanol bath. In these conditions, the NMR tube was opened to an atmosphere of 2 bar of NH_3 (g) for 10 min. During the first hours of reaction, the NMR spectra show formation of several species, which are in equilibrium. The NMR data of this system at different temperatures are the following (for more deails see the main text and Supporting Information, Figures S1 and S2): ^{11}B-{^1H} NMR (128 MHz; CD_2Cl_2; 298 K): δ +9.8, +8.9, +3.9, −2.9, −16.3, −17.7, −22.8, −24.6, −30.4. ^1H NMR (500 MHz; CD_2Cl_2; 298 K): δ +7.58 to +7.05 (aromatics, PPh_3), +3.61 (br s, BH), +3.52 (br s, BH), +3.31 (low intensity, br s, BH) +2.48 (br s, BH), +2.35 (br s, BH), +2.21 (low intensity, br s, BH), +1.58 (low intensity, br s, BH), +1.48 (br s, BH), +1.11 (br s, BH), +0.98 (br s, BH), +0.50 (high intensity 17-fold excess NH_3), −3.30 (br s, BHB), −3.53 (br s, BHB). ^1H NMR (500 MHz; CD_2Cl_2; 203 K): δ +7.60 to +6.31 (aromatics, PPh_3), +3.81 (br d, J = 17.8 Hz. BH), +3.63 (low intensity br s, BH), +3.50 (low intensity br s, BH), +3.31 (br s, BH), +3.17 (low intensity br s, BH), +3.03 (low intensity br s, BH), +2.41 (br s, BH), +2.02 (br s, BH), +1.50 (br s, BH), +1.46 (br s, BH), +1.29 (br s, BH), +0.92 (br s, BH), +0.65 (br s, BH), +0.51 (br s, BH), +0.47 (high intensity, excess of free NH_3), −2.92 (br s, BHB), −3.83 (low intensity br s, BHB), −4.07 (br s, BHB), −4.74 (br s, BHB). ^{31}P-{^1H} NMR (202 MHz; CD_2Cl_2; 298 K): δ + 37.6 (br d, J_{RhP} = 139 Hz), 37.4 (d, J_{RhP} = 144 Hz), +28.3 (s, O=PPh_3). ^{31}P-{^1H} NMR (202 MHz; CD_2Cl_2; 203 K): δ +40.7 (d, J_{RhP} = 142.2 Hz), +34.7 (dd, J_{RhP} = 137.4, $^2J_{PP}$ = 18.2 Hz), +25.2 (d, J = 119.7 Hz), +24.5 (dd, J_{RhP} = 121.1, $^2J_{PP}$ = 18.2 Hz), +25.4 (s, O=PPh_3), −7.9 (s, free PPh_3).

Table 3. Crystallographic Data and Structure Refinement Information for 2

chemical formula	$C_{36}H_{43}B_9NP_2RhS$
formula mass	783.91
crystal system	monoclinic
a/Å	12.4394(9)
b/Å	21.8740(16)
c/Å	14.4668(10)
α/°	90.00
β/°	110.5680(10)
γ/°	90.00
unit cell volume/Å^3	3685.5(5)
temperature/K	100(2)
space group	$P21/n$
no. of formula units per unit cell, Z	4
radiation type	Mo Kα
absorption coefficient, μ/mm^{-1}	0.636
no. of reflections measured	43702
no. of independent reflections	8787
R_{int}	0.0414
final R_1 values ($I > 2\sigma(I)$)	0.0389
final $wR(F^2)$ values ($I > 2\sigma(I)$)	0.0955
final R_1 values (all data)	0.0464
final $wR(F^2)$ values (all data)	0.1014
goodness of fit on F^2	1.087

dx.doi.org/10.1021/ic501779n | Inorg. Chem. 2014, 53, 12428−12436

After 40 h in solution, the sample evolves to the formation of **2** as a single product. The formation of **2** is quantitative by NMR spectroscopy. And, although we managed to obtain a crystal suitable for X-ray diffraction analysis, the lability of compound **2** precluded, in our hands, to isolate this hydridorhodathiaborane as an analytically pure sample. ^{11}B NMR (128 MHz; CD_2Cl_2; 298 K): orders as δ_B [calculated δ_B] +7.2 (2B, br s, B−H) [+9.5 B(3), +8.5 B(9)], +3.8 (1B, v br d, B−H) [+7.8 B(6)], −0.3 (1B, br d, J_{BH} = 137 Hz, B−H) [+0.1 B(4)], −3.5 (1B, s, B−H) [-0.3 B(11)], −13.1 (1B, d, J_{BH} = 143 Hz, B−H) [-13.3 B(5)], −18.4 (1B, s, J_{BH} = 129 Hz, B−H) [-21.9 B(10)], −25.9 (1B, s, J_{BH} = 137 Hz, B−H) [−25.1 B(1)], −30.8 (1B, v. br, B−H) [−29.0 B(2)]. ^{1}H−{^{11}B} NMR (300 MHz; CD_2Cl_2; 298 K): δ 8.03−6.42 (m, 1H, aromatics, PPh_3), +3.46 (1H, s, B−H), +3.35 (1H, s, B−H), +2.63 (1H, s, B−H), +2.50 (1H, s, B−H), +1.69 (1H, s, B−H), +1.31 (1H, s, B−H), +1.01 (1H, s, B−H), +0.81 (1H, s, B−H), +0.38 (1H, s, B−H), −2.50 (1H, br s, B−H−B), −12.54 (1H, apparent q, J_{RhH} + $2J_{PH}$ ≈ 18.7 Hz, Rh−H). ^{31}P-{^{1}H} NMR (161 MHz; CD_2Cl_2; 203 K): δ +38.6 (1P, dd, J_{RhP} = 130 Hz, $^2J_{PP}$ = 18 Hz, PPh_3), +29.8 (1P, br d, J_{RhP} = 95.8 Hz, $^2J_{PP}$ no observed due to the broadness of the peaks, PPh_3).

*[8,8,8-(NH$_3$)(PPh$_3$)$_2$-nido-8,7-RhSB$_9$H$_{10}$] (**4**).* A 55 mg (0.072 mmol) portion of **1** was dissolved in 7 mL of dichloromethane in a Young-type Schlenk tube. The system was degassed by three freeze−thaw cycles, after which it was cooled to the liquid nitrogen temperature and then pumped for several minutes. Immersed in a CO_2/isopropanol bath at −75 °C, the sample was exposed to 2 bar of NH_3 for 1 min. The color of the solution changed immediately from bright red to bright yellow. Mantaining the tube at low temperature, the CH_2Cl_2 yellow solution was overlaid with hexane, and the resulting system was immnersed in a CO_2/isopropanol at low temperatures for 4 days. After this time, a yellow precipitate formed. The supernatant was removed with a cannula under argon, to leave a yellow solid that was washed three times with hexane and dried in vacuum to give 11.6 mg of product. This product was characterized as [8,8,8-(NH_3)(PPh_3)$_2$-8,7-$RhSB_9H_{10}$] (**4**). Yield: 0.015 mmol, 20%. IR (ATR): v 3385m, 3360m, 3343m, and 3314m overlapping bands (NH), 3260m (NH), 3060vw, 2549vs (BH), 2489vs (BH), 2447vs (BH). ^{11}B-{^{1}H} NMR (160 MHz; CD_2Cl_2; 298 K): δ +15.4 (1B, s, BH), +10.7 (1B, s, BH), +7.0 (1B, s, BH), +2.4 (2B, s. BH), −11.6 (1B, s, BH), −19.5 (1B, s, BH), −20.5 (1B, s, BH), −29.1 (1B, s, BH): these signals resemble the values of pure compound **1**. Other peaks of small intensity were observed at δ_B +32.6, +31.7, −14.6, −23.6, −25.5, −31.4. ^{11}B-{^{1}H} NMR (160 MHz; CD_2Cl_2; 203 K): very broad signals as expected due to fast relaxation of the boron nuclei: δ +32.0, +9.4, +4.04, −2.8, −16.8, −23.0, −32.5. ^{1}H-{^{11}B} NMR (500 MHz; CD_2Cl_2; 298 K): δ +7.77 − +7.11 (30H, aromatics, PPh_3), +4.11 (1H, br s, BH), +3.41 (2H, br s, BH), +2.66 (1H, br s, BH), +1.71 (1H, br s, BH), +1.58 (1H, br s, BH), +1.22 (2H, br s, BH), +0.85 (3H, s, NH_3), −1.64 (1H, br s, BHB). ^{1}H NMR (500 MHz; CD_2Cl_2; 263 K): δ +7.71 − +7.06 (30H, aromatics, PPh_3), +3.72 (1H, br s, BH), +3.34 (1H, br s, BH), +3.22 (1H, br s, BH), +2.91 (1H, br s, BH), +2.19 (1H, br s, BH), +1.63 (2H, br s, BH), +1.47 (1H, br s, BH), +1.06 (1H, br s, BH), +0.90 (3H, s, NH_3), −3.11 (1H, br s, BHB). ^{1}H NMR (500 MHz; CD_2Cl_2; 203 K): δ +7.65 − +6.95 (28H, aromatics, PPh_3), +6.36 (2H, s, aromatic, PPh_3) +3.83 (1H, br s, BH), +3.32 (2H, br s, BH), +2.45 (1H, br s, BH), +2.021 (1H, br s, BH), +1.53 (1H, br s, BH), +1.35 (3H, s, NH_3), +0.96 (1H, br s, BH), +0.70 (1H, br s, BH), −4.64 (1H, br s, BHB). ^{31}P-{^{1}H} NMR (202 MHz; CD_2Cl_2; 298 K): δ + 41.4 (low intensity d, J_{RhP} = 163 Hz), +39.1 (d, J_{RhP} = 151 Hz, Rh−PPh_3), +27.5 (s, $OPPh_3$), +19.2 (v br s, Rh−PPh_3). ^{31}P-{^{1}H} NMR (202 MHz; CD_2Cl_2; 263 K): δ +41.8 (low intensity d, J_{RhP} = 139 Hz), +34.7 (br d, J_{RhP} = 144), +28.0 (s, $OPPh_3$), +23.0 (v br d, J = 128 Hz). ^{31}P-{^{1}H} NMR (202 MHz; CD_2Cl_2; 203 K): δ +41.9 (low intensity d, J_{RhP} = 142 Hz), +40.5 (low intensity d, J_{RhP} = 156 Hz), +34.9 (dd, J_{RhP} = 137 Hz, $^2J_{PP}$ = 18 Hz), +24.9 (dd, J_{RhP} = 121 Hz, $^2J_{PP}$ = 19 Hz). MS (ES$^-$, CH_3CN solvent): m/z 825 [M + CH_3CN]$^-$. Isotope envelope matches those calculated from the known isotopic abundances of the constituent elements.

■ ASSOCIATED CONTENT

Ⓢ Supporting Information

DFT-calculated coordinates; additional NMR spectra and cif for **2**. This material is available free of charge via the Internet at http://pubs.acs.org.

■ AUTHOR INFORMATION

Corresponding Author

*E-mail: rmacias@unizar.es.

Notes

The authors declare no competing financial interest.

■ ACKNOWLEDGMENTS

We acknowledge the Spanish Ministry of Economy and Competitiveness (CTQ2012-32095, CONSOLIDER INGENIO, CSD2009-00050, MULTICAT and CSD2006-0015, Crystallization Factory) for support of this work. The support from the KFUPM-University of Zaragoza research agreement and the Center of Research Excellence in Petroleum Refining & Petrochemicals at King Fahd University of Petroleum & Minerals (KFUPM) is also gratefully acknowledged. B.C. thanks the "Diputación General de Aragón" for a predoctoral scholarship. We thank Dr. Jonathan Bould for useful suggestions during this work.

■ REFERENCES

(1) (a) Klinkenberg, J. L.; Hartwig, J. F. *Angew. Chem., Int. Ed.* **2011**, *50*, 86. (b) Zimmermann, B.; Herwig, J.; Beller, M. *Angew. Chem., Int. Ed.* **1999**, *38*, 2372. (c) Gross, T.; Seayad, A. M.; Ahmad, M.; Beller, M. *Org. Lett.* **2002**, *4*, 2055. (d) Ogo, S.; Uehara, K.; Abura, T.; Fukuzumi, S. *J. Am. Chem. Soc.* **2004**, *126*, 3020. (e) Yamaguchi, R.; Kawagoe, S.; Asai, C.; Fujita, K.-I. *Org. Lett.* **2007**, *10*, 181. (f) Gunanathan, C.; Milstein, D. *Angew. Chem., Int. Ed.* **2008**, *47*, 8661. (g) Pouy, M. J.; Leitner, A.; Weix, D. J.; Ueno, S.; Hartwig, J. F. *Org. Lett.* **2007**, *9*, 3949. (h) Prinz, T.; Driessen-Hölscher, B. *Chem.—Eur. J.* **1999**, *5*, 2069. (i) Lavallo, V.; Frey, G. D.; Donnadieu, B.; Soleilhavoup, M.; Bertrand, G. *Angew. Chem., Int. Ed.* **2008**, *47*, 5224.

(2) Werner, A. *Z. Anorg. Allg. Chem.* **1893**, *3*, 267.

(3) (a) Hillhouse, G. L.; Bercaw, J. E. *J. Am. Chem. Soc.* **1984**, *106*, 5472. (b) Gunanathan, C.; Gnanaprakasam, B.; Iron, M. A.; Shimon, L. J. W.; Milstein, D. *J. Am. Chem. Soc.* **2010**, *132*, 14763. (c) Teltewskoi, M.; Kalläne, S. I.; Braun, T.; Herrmann, R. *Eur. J. Inorg. Chem.* **2013**, *2013*, 5762.

(4) (a) Casalnuovo, A. L.; Calabrese, J. C.; Milstein, D. *Inorg. Chem.* **1987**, *26*, 971. (b) Zhao, J.; Goldman, A. S.; Hartwig, J. F. *Science* **2005**, *307*, 1080. (c) Salomon, M. A.; Jungton, A.-K.; Braun, T. *Dalton Trans.* **2009**, 7669. (d) Klaring, P.; Pahl, S.; Braun, T.; Penner, A. *Dalton Trans.* **2011**, *40*, 6785. (e) Mena, I.; Casado, M. A.; García-Orduña, P.; Polo, V.; Lahoz, F. J.; Fazal, A.; Oro, L. A. *Angew. Chem., Int. Ed.* **2011**, *50*, 11735. (f) Mena, I.; Casado, M. A.; Polo, V.; García-Orduña, P.; Lahoz, F. J.; Oro, L. A. *Angew. Chem., Int. Ed.* **2012**, *51*, 8259. (g) Schulz, M.; Milstein, D. *J. Chem. Soc., Chem. Commun.* **1993**, 318.

(5) (a) Stock, A. *Hydrides of Boron and Silicon*; Cornell University: Ithaca, NY, 1933. (b) Shore, S. G. Ph.D. Dissertation, University of Michigan, 1956. (c) Parry, R. W. *J. Chem. Educ.* **1997**, *74*, 512. (d) Li, F.; Shelly, K.; Knobler, C. B.; Hawthorne, M. F. *Inorg. Chem.* **1999**, *38*, 4926. (e) Nordman, C. E.; Reimann, C. *J. Am. Chem. Soc.* **1959**, *81*, 3538. (f) Yoon, C. W.; Carroll, P. J.; Sneddon, L. G. *J. Am. Chem. Soc.* **2008**, *131*, 855. (g) Li, F.; Shelly, K.; Knobler, C. B.; Hawthorne, M. F. *Angew. Chem., Int. Ed.* **1998**, *37*, 1868. (h) Mebs, S.; Kalinowski, R.; Grabowsky, S.; Förster, D.; Kickbusch, R.; Justus, E.; Morgenroth, W.; Paulmann, C.; Luger, P.; Gabel, D.; Lentz, D. *Inorg. Chem.* **2010**, *50*, 90.

(6) (a) Armaroli, N.; Balzani, V. In *Energy for a Sustainable World*; Wiley-VCH Verlag GmbH & Co. KGaA, 2010. (b) Romm, J. J. *Der*

Wasserstoff-Boom; Wiley-VCH: Weinheim, 2006. (c) Baker, T. R. *Dalton Trans.* **2007**, 2613. (d) Chandra, M.; Xu, Q. *J. Power Sources* **2006**, *156*, 190.
(7) (a) Käß, M.; Friedrich, A.; Drees, M.; Schneider, S. *Angew. Chem., Int. Ed.* **2009**, *48*, 905. (b) Woon Yoon, C.; Sneddon, L. G. *J. Am. Chem. Soc.* **2006**, *128*, 13992. (c) Yang, X.; Hall, M. B. *J. Am. Chem. Soc.* **2008**, *130*, 1798. (d) Chaplin, A. B.; Weller, A. S. *Angew. Chem., Int. Ed. Engl.* **2010**, *49*, 581. (e) Douglas, T. M.; Chaplin, A. B.; Weller, A. S. *J. Am. Chem. Soc.* **2008**, *130*, 14432. (f) Clark, T. J.; Russell, C. A.; Manners, I. *J. Am. Chem. Soc.* **2006**, *128*, 9582. (g) Rossin, A.; Bottari, G.; Lozano-Vila, A. M.; Paneque, M.; Peruzzini, M.; Rossi, A.; Zanobini, F. *Dalton Trans.* **2013**, *42*, 3533. (h) Duman, S.; Ozkar, S. *Int. J. Hydrogen Energy* **2013**, *38*, 180. (i) Lu, Z.; Conley, B. L.; Williams, T. J. *Organometallics* **2012**, *31*, 6705. (j) Conley, B. L.; Guess, D.; Williams, T. J. *J. Am. Chem. Soc.* **2011**, *133*, 14212. (k) Staubitz, A.; Sloan, M. E.; Robertson, A. P. M.; Friedrich, A.; Schneider, S.; Gates, P. J.; Schmedt auf der Gunne, J.; Manners, I. *J. Am. Chem. Soc.* **2010**, *132*, 13332. (l) Kim, S.-K.; Han, W.-S.; Kim, T.-J.; Kim, T.-Y.; Nam, S. W.; Mitoraj, M.; Piekos, L.; Michalak, A.; Hwang, S.-J.; Kang, S. O. *J. Am. Chem. Soc.* **2010**, *132*, 9954. (m) Conley, B. L.; Williams, T. J. *Chem. Commun.* **2010**, *46*, 4815. (n) Boulho, C.; Djukic, J.-P. *Dalton Trans.* **2010**, *39*, 8893.
(8) Ferguson, G.; Jennings, M. C.; Lough, A. J.; Coughlan, S.; Spalding, T. R.; Kennedy, J. D.; Fontaine, X. L. R.; Stibr, B. *J. Chem. Soc., Chem. Commun.* **1990**, 891.
(9) (a) Álvarez, Á.; Macías, R.; Fabra, M. J.; Lahoz, F. J.; Oro, L. A. *J. Am. Chem. Soc.* **2008**, *130*, 2148. (b) Álvarez, Á.; Macías, R.; Bould, J.; Fabra, M. J.; Lahoz, F. J.; Oro, L. A. *J. Am. Chem. Soc.* **2008**, *130*, 11455.
(10) Orpen, A. G. *J. Chem. Soc., Dalton Trans.* **1980**, 2509.
(11) Wade, K. *Adv. Inorg. Chem. Radiochem.* **1976**, *18*, 1.
(12) McAnaw, A.; Scott, G.; Elrick, L.; Rosair, G. M.; Welch, A. J. *Dalton Trans.* **2013**, *42*, 645.
(13) Allen, F. *Acta Crystallogr.* **2002**, *58*, 380.
(14) Calvo, B.; Kess, M.; Macias, R.; Cunchillos, C.; Lahoz, F. J.; Kennedy, J. D.; Oro, L. A. *Dalton Trans.* **2011**, *40*, 6555.
(15) Alvarez, A.; Macias, R.; Fabra, M. J.; Martin, M. L.; Lahoz, F. J.; Oro, L. A. *Inorg. Chem.* **2007**, *46*, 6811.
(16) Coughlan, S.; Spalding, T. R.; Ferguson, G.; Gallagher, J. F.; Lough, A. J.; Fontaine, X. L. R.; Kennedy, J. D.; Stibr, B. *J. Chem. Soc., Dalton Trans.* **1992**, 2865.
(17) Otwinowski, Z.; Minor, W. Processing of X-ray diffraction data collected in oscillation mode. In *Methods in Enzymology*; Carter, C., Jr., Ed.; Academic Press: New York, 1997; Vol. *276*, pp 307−326.
(18) Blessing, R. H. *Acta Crystallogr.* **1995**, *A51*, 33.
(19) Sheldrick, G. M. *Acta Crystallogr.* **1997**, *A46*, 467.
(20) Sheldrick, G. M. *Acta Crystallogr.* **2008**, *A64*, 112.
(21) Frisch, M. J.; Trucks, G. W.; Schlegel, H. B.; Scuseria, G. E.; Robb, M. A.; Cheeseman, J. R., Jr.; Montgomery, J. A.; Vreven, T.; Kudin, K. N.; Burant, J. C.; Millam, J. M.; Iyengar, S. S.; Tomasi, J.; Barone, V.; Mennucci, B.; Cossi, M.; Scalmani, G.; Rega, N.; Petersson, G. A.; Nakatsuji, H.; Hada, M.; Ehara, M.; Toyota, K.; Fukuda, R.; Hasegawa, J.; Ishida, M.; Nakajima, T.; Honda, Y.; Kitao, O.; Nakai, H.; Klene, M.; Li, X.; Knox, J. E.; Hratchian, H. P.; Cross, J. B.; Bakken, V.; Adamo, C.; Jaramillo, J.; Gomperts, R.; Stratmann, R. E.; Yazyev, O.; Austin, A. J.; Cammi, R.; Pomelli, C.; Ochterski, J.; Ayala, P. Y.; Morokuma, K.; Voth, G. A.; Salvador, P.; Dannenberg, J. J.; Zakrzewski, V. G.; Dapprich, S.; Daniels, A. D.; Strain, M. C.; Farkas, O.; Malick, D. K.; Rabuck, A. D.; Raghavachari, K.; Foresman, J. B.; Ortiz, J. V.; Cui, Q.; Baboul, A. G.; Clifford, S.; Cioslowski, J.; Stefanov, B. B.; Liu, G.; Liashenko, A.; Piskorz, P.; Komaromi, I.; L.Martin, R.; Fox, D. J.; Keith, T.; Al-Laham, M. A.; Peng, C. Y.; Nanayakkara, A.; Challacombe, M.; Gill, P. M. W.; Johnson, B. G.; Chen, W.; Wong, M. W.; Gonzalez, C.; Pople, J. A. *Gaussian 03*; Gaussian, Inc: Wallingford, CT, 2004.